Ultrasonics Sonochemistry 95 (2023) 106400

Contents lists available at ScienceDirect

Ultrasonics Sonochemistry

journal homepage: www.elsevier.com/locate/ultson

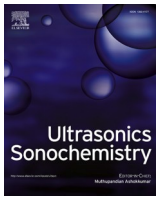

Inactivation of the enveloped virus phi6 with hydrodynamic cavitation

Mojca Zupanc [a], Jure Zevnik [a], Arijana Filipić [b], Ion Gutierrez-Aguirre [b], Meta Ješelnik [b], Tamara Košir [b], Jernej Ortar [a], Matevž Dular [a], Martin Petkovšek [a,*]

[a] Faculty of Mechanical Engineering, University of Ljubljana, Ljubljana, Slovenia
[b] Department of Biotechnology and Systems Biology, National Institute of Biology, Ljubljana, Slovenia

ARTICLE INFO

Keywords:
Enveloped viruses
Phi6
SARS-CoV-2
Virus inactivation
Hydrodynamic cavitation
Water decontamination

ABSTRACT

The COVID −19 pandemic reminded us that we need better contingency plans to prevent the spread of infectious agents and the occurrence of epidemics or pandemics. Although the transmissibility of SARS-CoV-2 in water has not been confirmed, there are studies that have reported on the presence of infectious coronaviruses in water and wastewater samples. Since standard water treatments are not designed to eliminate viruses, it is of utmost importance to explore advanced treatment processes that can improve water treatment and help inactivate viruses when needed. This is the first study to investigate the effects of hydrodynamic cavitation on the inactivation of bacteriophage phi6, an enveloped virus used as a SARS-CoV-2 surrogate in many studies. In two series of experiments with increasing and constant sample temperature, virus reduction of up to 6.3 logs was achieved. Inactivation of phi6 at temperatures of 10 and 20 °C occurs predominantly by the mechanical effect of cavitation and results in a reduction of up to 4.5 logs. At 30 °C, the reduction increases to up to 6 logs, where the temperature-induced increased susceptibility of the viral lipid envelope makes the virus more prone to inactivation. Furthermore, the control experiments without cavitation showed that the increased temperature alone is not sufficient to cause inactivation, but that additional mechanical stress is still required. The RNA degradation results confirmed that virus inactivation was due to the disrupted lipid bilayer and not to RNA damage. Hydrodynamic cavitation, therefore, has the potential to inactivate current and potentially emerging enveloped pathogenic viruses in water at lower, environmentally relevant temperatures.

1. Introduction

The 12 families of enveloped viruses (i.e., *Coronaviridae*, *Cystoviridae* (such as phi6), *Filoviridae*, *Hepadnaviridae*, *Herpesviridae*, *Orthomyxoviridae*, *Paramyxoviridae*, *Pneumoviridae*, *Poxviridae*, *Retroviridae*, *Rhabdoviridae*, *Togaviridae*) have been the cause of numerous epidemics and pandemics over the past decade [1]. Key examples include outbreaks of Ebola virus (EBOV), Zika virus (ZIKV), Dengue virus (DENV), hantaviruses, Lassa virus, and human respiratory viruses (e.g., coronaviruses (CoVs), influenza viruses) [2,3], while hepatitis B and C viruses continue to cause problems worldwide [2]. The severity of outbreaks has increased over the years, and the last one, caused by the severe acute respiratory syndrome coronavirus (SARS-CoV-2), affected the entire world in a way that modern society had not experienced before. The COVID-19 pandemic is currently in decline, but the world is still recovering, and fears of new global outbreaks of similar or even more contagious diseases have not yet dissipated.

The persistence of enveloped viruses in the aquatic environment and their transmission via water, including wastewater (WW) always raises concerns especially when dealing with highly infectious viruses such as Ebola virus and SARS-CoV-2 [3-8]. Even though enveloped viruses are usually not transmitted via water, the recent outbreak of SARS-CoV-2 has again sparked a heated discussion about different possible routes of their transmission [3,5,9,10]. Moreover, studies demonstrating new routes of viral particle transmission via water, such as adhesion to plastics, which could promote the survival and spread of enteric and respiratory viruses in water matrices [11], could only add fuel to the fire in the future. Although respiratory viruses are primarily airborne, some virus particles may still enter aquatic matrices via excretions, which is why studies on WW as a possible route of transmission have flourished

Abbreviations: EBOV, Ebola virus; ZIKV, Zika virus; DENV, Dengue virus; CoVs, coronaviruses; WW, wastewater; UV, ultraviolet; AC, acoustic cavitation; HC, hydrodynamics cavitation; PFU, plaque-forming units; DAL, double-layer agar assay; IT, increasing temperature; CT, constant temperature; Np, number of sample passes; R_v, log-reduction of virus concentration; •OH, hydroxyl radical; ROI, region of interest; fps, frames per second.

* Corresponding author.
E-mail address: martin.petkovsek@fs.uni-lj.si (M. Petkovšek).

https://doi.org/10.1016/j.ultsonch.2023.106400
Received 23 January 2023; Received in revised form 23 March 2023; Accepted 5 April 2023
Available online 11 April 2023

[6-8]. In the case of SARS-COV-2, these concerns likely stemmed from the fact that for some enveloped viruses like CoVs, influenza virus and Ebola virus, it has been reported that they can survive in various water/WW samples for long periods of time especially at lower temperatures [5-7,9,12], and from recently published data confirming faecal shedding of SARS-CoV-2 RNA from COVID-19 patients, which can last between 14 and 21 days [13-15]. If we consider that during an outbreak, the amount of virus particles in WW increases substantially, this may further increase the risk of their transmission through WW or other water sources that come into contact with WW [7,16].

Working with pathogenic viruses can be challenging as they pose a health risk to laboratory workers, so all work must be handled in laboratories with higher biosafety levels. As a result, scientists often resort to appropriate surrogates in their investigations. The bacteriophage phi6 is often used as a surrogate for enveloped viruses such as Ebola virus, influenza viruses, or CoVs [3,4,7,9], because of its similar size (~80–100 nm), and lipid envelope with spike proteins [17-19]. It has often been used as a surrogate for enveloped viruses to either learn about their fate in the environment under various conditions [3,4,9,20,21] or their susceptibility to inactivation by advanced treatment processes [7,18,21-23] or materials [19,24]. Due to their lipid bilayer, enveloped viruses are susceptible to inactivation by chemical agents [25-28] as well as harsher environmental conditions such as elevated temperatures [3,4,20,21] or high humidity [20,29]. They have also been successfully inactivated by UV [5,26] and advanced treatment processes such as photocatalysis, ozonation, and chlorination [5,26,30-32]. The same is true for phi6, which has been shown to be susceptible to inactivation by advanced treatments such as UV irradiation (200 – 320 nm) [7,18,23], IR radiation [22] and free chlorine [21,23].

Because the main route of enveloped viruses transmission is usually not through water, studies on inactivation of enveloped viruses in water and at lower temperatures are lacking [8]. However, the recent COVID-19 outbreak showed us that we must be prepared for the worst, as the emergence of enveloped viruses or virus strains that could be transmitted through water or WW is possible in the future. Current virus elimination methods all have some limitations: they are either expensive, time-consuming, require a large infrastructure (heat treatment at 95 °C, various filtrations and sedimentation), or, more importantly, they generate undesirable disinfection by-products that can be toxic in the long term (chlorination and UV light treatment) [33]. The only logical alternative, therefore, is to research and develop simple, environmentally friendly, economically feasible, robust, and easily scalable advanced technologies that could help us effectively and efficiently control potential future outbreaks, even at lower environmentally relevant temperatures. One such process with much potential is cavitation (hydrodynamic or acoustic).

Cavitation is a physical phenomenon that describes a phase transition from liquid to gas and back to a homogeneous liquid at approximately constant temperature. The effects of cavitation are in large part contributed to the bubble implosions. During the growth of cavitation bubble the energy is collected from the surrounding liquid, leading to bubble collapse in a very small spatiotemporal region, resulting in extreme mechanical effects (e.g. extreme shear forces, shock waves, pressure pulsations, high temperatures and micro jets) [34,35]. These result in decomposition of water molecules into species with high oxidation potential, especially $^{\bullet}$OH, $^{\bullet}$H which drive the chemical effects of cavitation [34]. Destruction of enveloped viruses could occur by two routes: (i) mechanical and thermal or (ii) chemical - $^{\bullet}$OH formed at the interface between the bubble and the surrounding area. There are some data describing virus inactivation by cavitation, but the exact mechanisms are not yet clear. For example, Su et al. [36] suggested that the damage caused during acoustic cavitation (AC) to the outer protein capsid itself or to recognition sites on the capsid surface may be the reason for the inactivation of the non-enveloped viruses studied (bacteriophage MS2, murine norovirus MNV-1, and feline calicivirus FCV-F9). In another study using hydrodynamic cavitation (HC), Kosel et al. [37] suggested that $^{\bullet}$OH, together with mechanical effects, could be responsible for MS2 inactivation by affecting the viral capsid or genome. Filipić et al. [38] used similar HC reactor to treat potato virus Y (PVY). Their results suggest that mechanical effects involved in PVY inactivation most likely involve high-pressure gradients at the transition of shockwaves generated during bubble collapse in HC. However, studies addressing the inactivation of enveloped viruses with HC are lacking. To the authors' knowledge, this is the first study on inactivation of any enveloped virus by HC.

Because it has been shown that MS2 and PVY, both non-enveloped viruses, can be successfully inactivated with HC in a Venturi constriction [37,38], the same device was chosen to investigate whether it can also effectively inactivate enveloped viruses. Therefore, the objectives of this study were to determine: i) whether HC can inactivate bacteriophage phi6 virus, ii) which HC effects, chemical or mechanical, are predominately responsible for its inactivation, and iii) whether sample temperature plays a role in the inactivation.

2. Materials and methods

2.1. Water samples

Water samples were inoculated with bacteriophage phi6 (DSM 21518) to a final concentration of 10^6 –10^7 plaque-forming units (PFU)/mL. Prior to each treatment, the pH of the samples was lowered with HCl and ranged from 4.8 to 5.8 for the purpose of the assessment of virus inactivation due to reasons discussed in Section 2.4. Assessment of virus inactivation. For experiments in HC test rig with either Venturi or control constriction, 1 L of tap water was prepared, while 100 mL of water was prepared for controls that included just stirring or incubation.

2.2. HC device and cavitation characterization

The HC test rig (Fig. 1), first described by Zupanc et al. [39], consisted of two reservoirs (1), each with a volume of 2 L, connected by a symmetrical Venturi double inclined constriction (2) made of transparent acrylic glass. The described device is operated with compressed air and an UNI-AIR automated 5/3 way double sided pneumatic valve (3) via National Instrument (NI) measurement card USB-6002, and NI Labview software. Once the sample is introduced into the first reservoir, the pressure difference between the reservoirs pushes the liquid through the Venturi with a height of 1 mm and a width of 5 mm, behind which cavitation forms due to the created low-pressure region. In addition to the original design [39], a cooling coil (4) was installed in the reservoir connected to an external cooling unit Polyscience - DuraChill CA03 with 1.28 kW cooling capacity (5) to maintain the desired temperature of the sample. The temperature was monitored by a built-in 4-wire Pt100 resistance temperature sensor (6). Liquid level switches – Materm NS120 (7) were also installed in both reservoirs to precisely control the pneumatic valve when switching the direction of the pressure difference between the vessels to change the direction of the liquid flowing through the Venturi constriction.

Sample volume of 1 L and a pressure difference of 7 bar between the reservoirs, were kept constant for all experiments performed in HC test rig with Venturi constriction. The passage through the Venturi constriction (Fig. 1: A) lasted 4.5 s and is defined as one cavitation pass. Control experiments, in which the Venturi constriction was replaced by a non-cavitating test section - control constriction (Fig. 1: B) made of the same material as the Venturi constriction, were performed with a 1.2 bar pressure difference, resulting in a duration of 9 s for a single Np. Also here, the sample volume was 1 L. The control experiments were designed to determine whether virus inactivation was due to factors other than HC. Operating conditions for both Venturi and control test sections are gathered in Table 1, where Reynolds and cavitation numbers are calculated as:

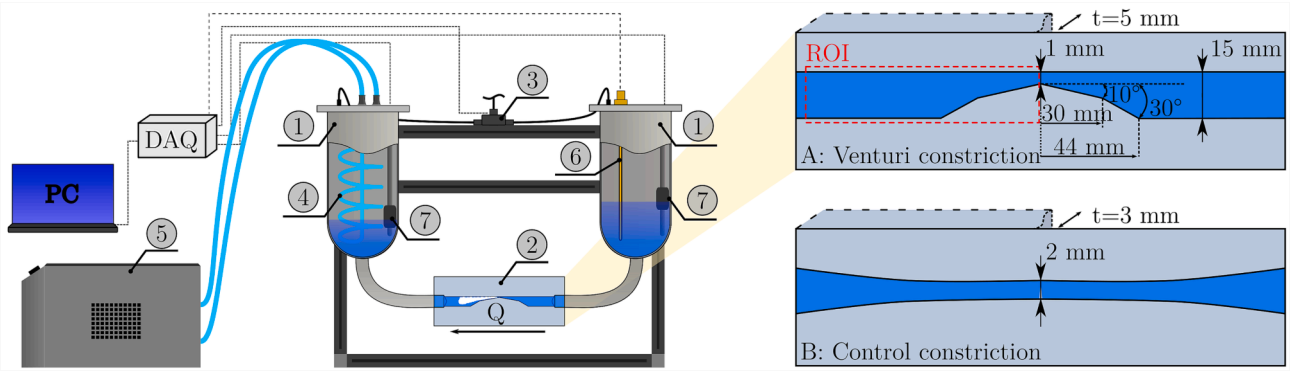

Fig. 1. Experimental setup scheme with visible HC test-rig elements (left): (1) reservoirs, (2) Venturi constriction, (3) 5-way pneumatic valve, (4) cooling coil, (5) cooling unit, (6) thermometer Pt100 and (7) level sensor. Dimensions of the Venturi (A) and control constriction (B) are presented on the scheme on the right. ROI - region of interest.

Table 1
Operating conditions for HC and control runs.

Experimental run	HC	Control
Test section geometry	Venturi constriction	Control constriction
Cross section at the narrowest part (mm × mm)	1 × 5	2 × 3
Pressure difference (bar)	7	1.2
Time for a single pass (s)	4.5	9
Flowrate (L/min)	13.3	6.7
Top velocity (m/s)	44.4	18.5
Reynolds number ()	6×10^5	2×10^5
Cavitation number ()	0.8	1.3

$$Re = \frac{u \bullet L}{\nu}, and \sigma = \frac{p_0 - p_v}{\frac{1}{2}\rho u^2}$$

with u as velocity, L as channel cross section perimeter, ν as kinematic viscosity, p_v as vapour pressure and ρ as density.

Cavitation characterization was performed using the high-speed visualisation method. We used Photron Fastcam SA-Z at a frame rate of 90,000 fps and resolution of 1024 × 208 pixels. Region of interest (ROI) is marked by red dashed rectangle on Fig. 1. Backlight illumination with high power LED lamp allowed a shutter time of 1 μs, with medium opened aperture on a 105 mm Nikkor lens.

2.3. Experimental design

In the present study, the effect of sample temperature alone or in combination with HC on the enveloped bacteriophage phi6, was investigated. Firstly, the effectiveness of the HC device was investigated under increasing (IT) and constant temperature (CT). During the IT experiments (Table 2: HC – IT, HC + M – IT30), when cooling was turned off, the temperature of the samples rose from initial 11.2 °C ± 0.8 °C up to 30.1 °C ± 1.5 °C. In the Exp. V6* 1 mL/L of methanol [38], known •OH scavenger was added, to determine whether the virus is susceptible to the •OH formed during HC. In addition, the effect of scavenger alone on the virus was investigated in a beaker under constant stirring (Table 2: Exp. S2*). During the CT experiments (Table 2: HC – CT) temperature was maintained constant at 10, 20 and 30 °C ± 1 °C. To determine the effect of temperature on virus inactivation, we performed 3 sets of control experiments (Table 2: C – IT20, C – IT30, C – CT). In the

Table 2
Experimental design.

Exp.	Exp. set	HC	T (°C)	Sampling after Np							HC constriction	Pressure difference
				0	60	125	250	500	750	1000		
V1	HC – IT30	+	IT30	+	+	+	+	+	–	–	Venturi	7 bar
V2		+		+	+	+	+	+	–	–	1 × 5 mm	
V3		+		+	+	+	+	+	–	+		
V4		+		+	+	+	+	+	–	+		
V5		+		+	+	+	+	+	–	+		
V6*	HC + M – IT30	+		+	+	+	+	+	–	+		
V7	HC – CT	+	CT: 10	+	+	+	+	+	+	+		
V8		+	CT: 20	+	+	+	+	+	+	+		
V9		+	CT: 30	+	+	+	+	+	+	+		
C1	C – IT20	–	IT20	+	+	+	+	+	–	–	Control	1.2 bar
C2		–		+	+	+	+	+	–	+	2 × 3 mm	
C3		–		+	+	+	+	+	–	+		
C4		–		+	+	+	+	+	–	+		
C5	C – IT30	–	IT30	+	+	+	+	+	–	+		
C6		–		+	+	+	+	+	–	+		
C7		–		+	+	+	+	+	–	+		
C8	C – CT	–	CT: 10	+	+	+	+	+	+	+		
C9		–	CT: 20	+	+	+	+	+	+	+		
C10		–	CT: 30	+	+	+	+	+	+	+		
S1	–	–	CT: 30	+	+	+	+	+	+	+	Stirrer	
S2*		–	RT	+	–	–	–	+	–	+		
0		–	CT: 33	+	+	+	+	+	+	+	Incubation	

V: Venturi; *: addition of methanol (M); C: control; S: magnetic stirrer; 0: incubation experiment; HC: hydrodynamic cavitation; IT: increasing temperature; CT: constant temperature; RT: room temperature; IT20: increasing temperature up to 20 °C; IT30: increasing temperature up to 30 °C; Np: number of HC passes; +: sample collected; -: sample not collected.

first set (Table 2: C – IT20), the temperature was allowed to increase uncontrolled up to 20 °C. In the second set (Table 2: C – IT30), the temperature increase was controlled to imitate the increase during HC experiments up to 30 °C. The final set of control experiments was performed at CT (Table 2: C – CT) of 10, 20 and 30 °C. We performed two additional experiments to assess the influence of the T and/or stirring on the virus infectivity: incubation at 30 °C in a beaker under constant stirring (Table 2: Exp. S1) and same incubation at 33 °C but without stirring (Table 2: Exp. 0). The treatment times equalled to the number of cavitation passes (Np) of HC treatments.

For all experiments performed in the HC device, 10 – 12 mL of representative aliquots were collected after 0, 60, 125, 250, 500, 750, and 1000 Np, depending on the experiment (Table 2), whereas for experiments performed on the magnetic stirrer, 4 – 5 mL of representative aliquots were collected after times corresponding to these Np. A smaller portion of each aliquot was taken for further PCR analysis and stored at −80 °C. pH was measured before and after every sampling using a Hach-Lange multimeter HQ430d and Intellical PHC725 probe. At the beginning of the experiments, pH ranged from 5 to 5.5 and rose for approximately 1.5 during the experiments, to around 6.5 – 7 at the end (Supporting information Table S1).

2.4. Quantification of infective phi6 with double-layer agar (DAL) assay

In order to assess the virus inactivation, the concentration of infective viruses before and after treatments was determined using double-layer agar assay (DAL) as described in [40]. In the initial HC experiments we observed that the pH of water containing phi6 increased after cavitation treatments from ~ 7.5 to 8.3 after 500 or more Np. This increase in pH affected the linearity in the dilutions used for phi6 (PFU/ml) quantification with DAL through an underestimation of the plaque count in samples taken at higher Np (higher pH), which led to an overestimated inactivation. This effect was likely triggered by aggregation of bacteriophages at pH above pH 7.5, which made difficult to pipette a representative viral population at non diluted concentrations. This was confirmed with experiments where we lowered the initial pH using HCl. In those experiments the pH never exceeded 7.4 and the linearity in the dilutions for quantification was optimal. Use of buffering to keep pH constant was avoided as any additives can influence the cavitation process, as was shown in one of our previous studies [41]. Therefore, for all further experiments included in this study, the initial pH was lowered (as described in Section 2.1), which did not affect the infectivity of the virus nor the cavitation process.

2.5. RNA degradation

To examine the effects of HC on viral RNA degradation, longer fragment reverse transcription (RT)–PCRs were performed for the experiments treated in the HC device at CT (e.g., Exp. V7, V8, V9, C8, C9, C10). First, RNA was extracted using the QIAmp Viral RNA Mini Kit (Qiagen) according to the manufacturer's instructions, with minor modifications, including the final elution step with 45 μL RNase-free water. A sample of RNase-free water was included in each extraction round as a negative control to exclude possible contamination during extraction.

Extracted RNA was amplified using RT–PCR with two primer sets (~1200 bp), L1 and L2 (Table 3), targeting two regions of one of three phi6's genomic segments (e.g. Large, Medium, Small), namely the large genome segment. Primer sequences were designed using primer- BLAST (NSBI, USA). For the preparation of the RT–PCR mixture, the OneStep RT–PCR kit (Qiagen, Germany) was used without the Q solution, according to the manufacturer's instructions, with minor modifications including smaller reaction volumes of 25 μL, which contained 5 μL of template RNA. Cycling conditions were: 30 min at 50 °C, 15 min at 95 °C, 35 cycles of 30 s at 94 °C, 60 s at 58 °C and 120 s at 72 °C, 10 min at 72 °C, and an infinite hold at 4 °C. A non-template control, i.e., sterilized water, was included in each PCR run to monitor for possible contaminations of reagents during preparation of the PCR mixtures. Amplified PCR products were detected by 1 % agarose gel electrophoresis and visualized with ethidium bromide. The size of PCR products was estimated using a 1 – kb ladder. RNA was considered degraded if there was a noticeable difference in the intensity of the bands of both targets after the selected treatment time compared with the corresponding bands at time 0.

Table 3
Primer sequences used for RT–PCR.

Primer names	Length of amplified product (bp)	Position in the L genomic segment	Primer sequences
L1_F	1203	327–346	5′ TTCACTGCTCGCTCGTTTCT 3′
L1_R		1529–1510	5′ ATTTGGTGGAGCTGGTAGGC 3′
L2_F	1217	1903–1922	5′ TGCGTCGCTACTGACGTATC 3′
L2_R		3119–3100	5′ CAACGAACCACCTTGCTTGG 3′

F: forward; R: reverse.

2.6. Statistical analysis

To determine whether there exist statistically significant differences in the obtained viral inactivation between different experimental runs, a two-sample Kolmogorov-Smirnov test was conducted for each pair of HC treatment and its corresponding control run.

The effectiveness of HC in relation to control treatment was further quantified by linear regression of the obtained viral log reduction in the following manner:

$$R_v = k^* R_{v,control}$$

where R_v and $R_{v,control}$ denote the log reduction of virus concentration for HC treatment and control treatment, respectively. The intercept term is presently omitted, since initially (Np = 0) there is no virus inactivation to be expected. Regression coefficient k thus serves as the only fitting parameter, which can be understood as a measure of efficiency of HC treatment in comparison to the control treatment, e.g., the value of $k = 2$ would indicate a one-fold increase in the rate of virus inactivation when HC treatment is considered with respect to the control.

3. Results

3.1. Increasing sample temperature

The obtained results for experiments with IT (Table 2: Exp. sets HC – IT30, HC + M – IT30, C – IT20, and C – IT30) are gathered in Fig. 2, while the corresponding data are given in tabular form in the Supporting information (Tables S2 and S3). We observed that the reduction of virus concentration, Rv (measured in $\log_{10}$ plaque forming units (PFU)/mL) during the HC runs (Table 2: Exp. set HC – IT30) follows an increasing trend with the Np and reaches a peak of $R_v = 5.87 \pm 0.33$ at Np of one thousand (Fig. 2 – left, solid blue line). The sample temperature during the HC runs gradually increased from the initial 11.2 ± 0.9 °C to 29.7 ± 1.0 °C at 500 Np, and then remained almost constant until the end (Fig. 2 – right, solid blue line). The occurrence of a gradual sample heating is not surprising, as a constant flux of mechanical energy that drives water flow through the system ultimately dissipates into heat. The system eventually reaches a new equilibrium point, which is also a reason for sample temperature staying practically constant at approximately 30 °C beyond 500 Np. During control experiments with temperatures reaching ~ 20 °C (Table 2: Exp. set C – IT20) the sample underwent heating

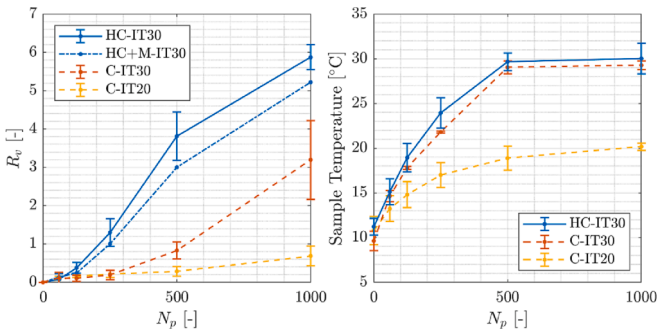

Fig. 2. Reduction of virus concentration (log10 PFU/mL, Rv) (**left**) and sample temperature (**right**) in relation to the number of passes (Np) through Venturi (Table 2: Exp. sets HC – IT30 and HC + M – IT30) and control (Table 2: Exp. sets C – IT30 and C – IT20) constrictions. Shown data are mean ± s.d. of each experimental set. The mean initial (Np = 0) virus concentrations were between 3×10^6 PFU/mL and 10×10^6 PFU/mL, which corresponds to log-values between 6.5 and 7.0.

with a slower rate due to a smaller expenditure of mechanical energy to drive flow in a control setup (Fig. 2 – right, yellow dashed line). For this reason, an additional set of control experiments was performed (Table 2: Exp. set C – IT30; Fig. 2 – right, orange dashed line), where sample temperature was controlled to match the ones from the HC runs, therefore reaching ~ 30 °C. Additionally, experimental set with the addition of methanol (Table 2: Exp. set HC + M – IT30) is included in Fig. 2 (left, blue dotted line).

Comparing the R_v of 5.87 ± 0.33 for HC runs with R_v of 0.69 ± 0.26 (Np = 1000) for control experiments with sample temperatures increasing until roughly 20 °C (Table 2: Exp. sets HC – IT30 and C – IT20; Fig. 2 – left, solid blue and dashed yellow line), one can observe a large difference of roughly 5-log reduction. However, we can also observe a R_v of 3.2 ± 1.0 (Np = 1000) for control runs (Table 2: Exp. set C – IT30; Fig. 2 – left, dashed orange line) with the matched sample temperature increase to the HC runs, which lowers the difference towards the HC run below 3-log reduction. A more detailed consideration of the obtained results reveals an uneven rate of virus reduction through time, which can be deducted from a non-linear relation between the Np and R_v (Fig. 2 - left, solid blue line). From there, two regions can be observed: an initially slow response with a gradual increase in virus inactivation rate between Np of 0 and 500, which is then again decelerated between Np of 500 and 1000. A similar accelerating trend can be also observed for the corresponding control runs (Table 2: Exp. set C – IT30; Fig. 2 – left, orange dashed line), which reach virus inactivation rate of roughly 4.7-log per 1000 sample passes between Np of 500 and 1000.

Two additional control runs were performed to ensure that phi6 virus remains viable at 30 °C in the absence of external mechanical loads. Solely incubation at 33 °C (Table 2: Exp. 0) and mixing on a magnetic stirrer at 30 °C (Table 2: Exp. S1) did not affect the virus infectivity. The obtained log reduction at exposure times equivalent to 1000 Np was 0.04 and 0.14, respectively (Supporting information Table S2).

3.2. Constant sample temperature

To further determine the effect of temperature on phi6 inactivation, additional HC experimental runs were conducted (Table 2: Exp. set HC – CT), where sample temperature was controlled and held constant at approximately 10, 20, and 30 °C. The corresponding data in tabular form are given in Supporting information Tables S2 and S3. The obtained results are gathered in Fig. 3, where R_v is shown in relation to the Np through a Venturi constriction (Fig. 3 – left, solid lines). These results show a more evenly increasing trend with Np. Additionally, we can observe a consistent increase in virus inactivation rate with higher sample temperature across all data points. For example, the final log reduction at 1000 Np amounts to 3.5 log, 4.5 log, and 6.3 log, for the cases with sample temperatures of 10, 20, and 30 °C, respectively. All these observations generally confirm the previous hypothesis of virus inactivation rate being temperature dependent.

Further statistical analysis (see Section 2.6) reveals that HC treatment (Table 2: Exp. set HC – CT) exhibits a significantly higher effectiveness at virus inactivation in comparison to the control treatment (Table 2: Exp. set C – CT) at sample temperatures of 10 and 20 °C (p-value 0.038). However, the same cannot be said for both treatments at sample temperature of 30 °C. There, the results suggest no difference between the HC and control treatment (p-value 0.44). The effectiveness of HC in relation to control treatment was further quantified by linear regression of viral log reduction Rv (see Section 2.6). Results (Fig. 3 – right and Table 4) show that HC at 10 °C and 20 °C presents with a roughly 7- and 3-fold virus inactivation effectiveness of the control experiments. Furthermore, the differences seem to be greater at lower

Table 4
Virus inactivation effectiveness of HC (Table 2: Exp. set HC – CT) in comparison to the control (Table 2: Exp. set C – CT) treatment. Results of the fitted linear model are presented for three different sample temperatures. Coefficient *k* can be understood as a measure of HC treatment effectiveness in comparison to the corresponding control. Subscript of k denotes the sample temperature.

Temperature	Coefficient *k*	Value	95 % conf. int.	R-squared
10 °C	k_{10}	7.20	[5.70,8.70]	0.91
20 °C	k_{20}	3.02	[1.85,4.18]	0.70
30 °C	k_{30}	1.06	[0.88,1.24]	0.88

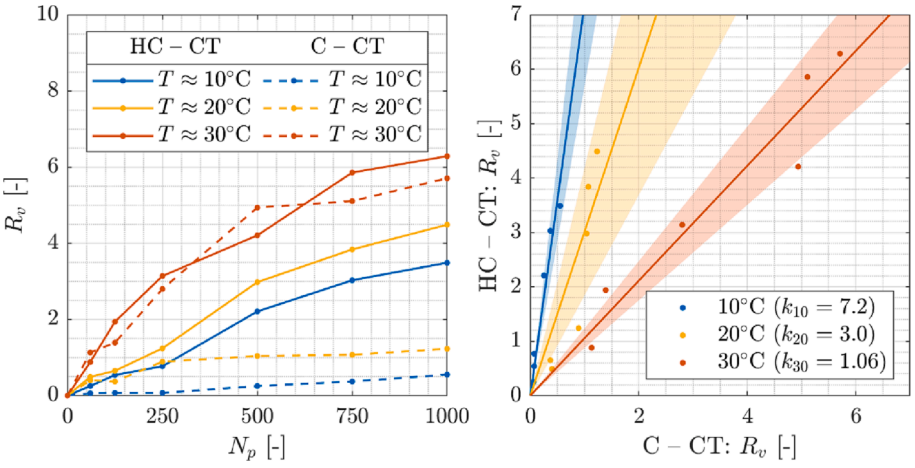

Fig. 3. Left: Reduction of virus concentration (log_{10} PFU/mL, Rv) in relation to the number of sample passes (Np) through Venturi (solid lines, Table 2: Exp. set HC – CT) and control (dashed lines, Table 2: Exp. set C – CT) constrictions. The initial (Np = 0) virus concentrations were 6.4×10^6 PFU/mL ± 4.9×10^6 PFU/mL and 4.4×10^6 PFU/mL ± 4.3×10^6 PFU/mL for HC and control experiments, respectively. **Right:** HC treatment (Table 2: Exp. set HC – CT) effectiveness in comparison to the control (Table 2: Exp. set C – CT) at constant sample temperatures of 10 °C (blue), 20 °C (yellow), and 30 °C (orange). A linear model (solid line) is fitted to the data (dots). The 95 % confidence intervals of the obtained regression coefficients *k* are denoted by a coloured fill. (For interpretation of the references to colour in this figure legend, the reader is referred to the web version of this article.)

temperatures and disappear at 30 °C.

Despite high viral inactivation after some treatments, results from RT-PCR showed no degradation of viral RNA after HC (Table 2: Exp. set HC – CT) and control (Table 2: Exp. set C – CT) treatments at constant temperature.

In addition, high-speed visual visualization of HC in a Venturi constriction was performed to evaluate whether the developed cavitation characteristics are affected at water temperatures between 10 °C and 30 °C. Fig. 4 presents typical cavitation sequences with 1 ms time resolution in water at 10, 20, and 30 °C. The water flows from right to left in all three cases. As can be seen, there are no major differences in the macroscale cavitation structures, including their magnitude and dynamics. In all three cases, cavitation is fully developed with intense cloud shedding. When cavitation is fully developed (t_i), the cloud begins to detach from the main cavitation structure ($t_i + 1$ ms) and collapses (approximately at $t_i + 3$ ms) downstream from the Venturi throat. This results in a few rebounds and produces a large number of individual vapor–gas bubbles ($t_i + 4$ ms, $t_i + 5$ ms) ahead of the newly developing cavitation cloud, which again reaches its maximum size at $t_i + 6$ ms. Concentration of methanol used in this study did not change cavitation dynamics in general, which was already confirmed in our previous study [38] by high-speed visualization. Additional cavitation comparison is included in the Supporting information Fig. S4.

4. Discussion

Results show that the rate of virus inactivation R_v is not constant during HC – IT experiments (Table 2: Exp. set HC – IT30; Fig. 2 – left, blue solid line). Two distinct regions of inactivation rates can be observed. In the first region (Np = 0 – 500) the rate of R_v increases as the sample temperature rises from 10 to 30 °C, while in the second region (Np = 500 – 1000) the R_v rate slows down and the temperature remains constant at 30 °C. The first set of control experiments (Table 2: Exp. set C – IT20; Fig. 2 – left, yellow dashed line) implied that the presence of HC is necessary to achieve substantial virus inactivation in both regions. The results achieved in the first region can be to some extent explained by the observations during CT experiments, where higher R_v was determined at higher temperatures (Fig. 3). Whereas the results achieved in the second region could be due to a decrease in the probability of viruses coming into the proximity of destructive hydrodynamic forces when the remaining viable virus concentration becomes sufficiently small. The results suggested that there must be a significant change in either cavitation conditions and/or viral susceptibility to the cavitation treatment during IT experiments. Since in our case the temperature increased with Np, this could influence both. It is known that cavitation dynamics and erosion potential are temperature dependent, where increase of cavitation extent with increasing temperature occurs due to changes in vapor pressure [42,43]. In our case, however, the difference in temperature between 10 °C and 30 °C does not change the vapor pressure significantly, and thus no major changes in visualization of cavitating flow with high-speed camera (Fig. 4) were noticed. For this reason, it is highly unlikely that even if the micro changes in cavitation dynamics (below the visualization threshold) did occur, they would be the primary reason behind the observed inconsistencies in R_v rate after 500 Np. This was additionally confirmed by the second set of control experiments (Table 2: Exp. set C – IT30; Fig. 2 – left, orange dashed line), which imitated the temperature trend observed in HC experiments. From Fig. 2 it can be deducted, that once the temperature reaches a certain value (between 20 and 30 °C) it makes the virus more susceptible to inactivation by cavitation (Table 2: Exp. sets HC – IT30 and HC + M – IT30) or mechanical loads in absence of HC (Table 2: Exp. sets C – IT30 and C – IT20). The same R_v trend between HC – IT30 and C– IT30 after 500 Np confirms this. To determine if OH radicals are involved in phi6 inactivation during IT experiments we performed an additional experiment with a radical scavenger (Table 2: Exp. set HC + M – IT30). We found no statistically significant differences in virus inactivation between experimental sets HC-IT30 and HC + M–IT30 (Fig. 2 – left, blue solid and dashed line), as a two-sample Kolmogorov-Smirnov test for mean R_v along Np yields a p-value > 0.99. Thus, we can deduce that $^{\bullet}$OH do not have a prominent role in the phi6 inactivation. Based on this, the observed phi6 inactivation is most probably due to mechanical effects of HC, which was determined also in our previous study regarding potato virus Y [38]. After 250 Np, when the sample's temperature increases, a slight decrease in virus inactivation can be seen, indicating that $^{\bullet}$OH might play a role. However, further, more detailed studies are needed to confirm this.

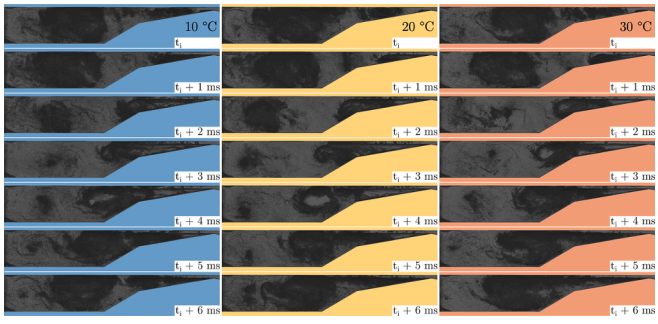

Fig. 4. High-speed visualization of cavitation in Venturi constriction at water temperature of 10, 20 and 30 °C.

Constant temperature experiments (Fig. 3) clearly corroborate the importance of temperature in phi6 inactivation. Data from the existing literature show that temperature can significantly affect the phase, i.e., liquid or gel, and mechanical characteristics of lipid bilayers. These together with glycoproteins comprise the membrane of enveloped viruses and play an important role in their resistance to environmental temperature changes [44]. For example, it was shown that phase change of the lipid bilayer of the influenza virus envelope to a gel phase occurs below 22 °C, which helps them withstand low environmental temperatures [45]. Similarly Morris et al. [29] showed that SARS-CoV-2 survives the longest at low temperatures and extreme relative humidity. Furthermore, Rath et al. [44] reported that the dynamics of the protein-membrane system of SARS-CoV-2 changes significantly between 30 and 40 °C. At 41 °C when the lipids transition from gel to liquid crystalline state their disorderliness increases, which also affects the M−protein embedded in the lipid membrane. Increased susceptibility to inactivation at higher temperatures was also shown for phi6 [3,20]. These data indicate that higher temperature is important for increased susceptibility of enveloped viruses to inactivation, which was also shown in our study. In HC – CT the lowest phi6 reduction of around 3-log occurred at 10 °C, approximately 1-log higher one was achieved at 20 °C, while around 6-log reduction can be observed at the highest investigated temperature of 30 °C (Fig. 3). The C – CT at 10 and 20° C clearly show that HC is the one responsible for the observed inactivation at these temperatures. Based on the result from the IT experiments with methanol (Table 2: HC + M – IT30), we speculate that mechanical effects of cavitation are the reason. This finding also corresponds well with the recent experimental and numerical research on cavitation bubble interaction with liposomes [46,47] and bacteria [48,49], where it was shown, that microstreaming is the primary mechanical driver of liposome deformation and bacterial cell damage, and that poration of cell membranes could be explained solely by mechanical effects.

At 30 °C in comparison to 10 °C and 20 °C, the inactivation of phi6 was noticeably higher, which can be due to the changes in virus' lipid bilayer due to elevated temperature. C – CT experiments clearly show that the effects of HC only play an important role at 10 and 20 °C, as the achieved phi6 inactivation at 30 °C in HC and control experiment was practically the same (Table 2: Exps. V9 and C10). Nevertheless, control experiments (Table 2: Exps. 0 and S1) revealed that a certain magnitude of mechanical load is still necessary to cause viral inactivation at around

30 °C as shown in control runs C – IT30 and C – CT30. This could be attributed to the different magnitude of hydrodynamic forces between the magnetic stirrer and control constriction. S1 experiment indicates that even though the viral lipid bilayer is weakened at 30 °C, this is still not sufficient to cause inactivation unless mechanical input, harsher than present under constant stirring, is applied. These however are not the well-known raw mechanical effects generated due to cavitation bubble collapses like thermal hot spots, shock waves, and bubble jetting, but milder ones like hydrodynamic forces in the form of local shear and pressure forces, which are also present in the control HC constriction. The slightly lower inactivation observed in experiment V6* (Fig. 2 – left, blue dotted line) also indicates that when cavitation is present, the changes that elevated temperature leaves on the virus envelope, open the way for both mechanical and chemical effects of cavitation. The weakened envelope could also be more susceptible to radical attack in addition to mechanical forces. In other studies, investigating the inactivation of phi6 under various advanced treatments different modes of action have been reported. The proposed mechanisms mostly revolve around the disruption of the viral lipid bilayer [17,19], damage to genome and membrane proteins [3,18,23], and oxidation of proteins in the nucleocapsid or polymerase complex [23], which all affect the viral infectivity. It seems that the chemical oxidants like chlorine mostly affect the viral proteins [23] while in the case of virus contact with different surfaces or advanced materials [17,19] the lipid envelope is the one affected. In this study, no damage was observed in the viral RNA. This, and the fact that mechanical effects were crucial for inactivation, suggest that the damage invoked on the lipid bilayer was the main cause of the virus inactivation.

Studies dealing with the behavior of enveloped viruses in WW effluents indicate that the inactivation of enveloped viruses is always slower at 20 °C and increases at 30 °C. Casanova et al. [4] showed that at 30 °C it takes 48 h to reach 5-log reduction of phi6, whereas 6 days are necessary to reach the same degree of reduction at 22 °C. Since the average yearly temperature of WW is around 15–20 °C (data for the EU), having a treatment technology available that can inactivate enveloped viruses, if the need arises, also at these temperatures, is very important. In addition to WW, this technology could also be applied for the treatment of other water sources. Our results clearly show that the effects of HC are the primary drivers of phi6 inactivation at lower sample temperatures (10 and 20 °C). Therefore, HC has a potential to become an advanced treatment of choice for inactivation of enveloped viruses in various water matrices. Even though our experiments were performed in tap water, they could be an indicator of what might happen to enveloped viruses in WW under HC treatment. Even more, higher degree of inactivation can be expected in more complex matrices due to the presence of other constituents that can accelerate the inactivation, such as enzymes [21]. We are aware that the presently employed treatment times (Np = 1000) are still far beyond feasible for real-world applications. Nevertheless, we see this as a challenge for our further studies and not as a setback.

5. Conclusions

The present study reports the inactivation of a phi6 virus commonly used as a surrogate for several enveloped viruses, including coronaviruses. At the beginning of the COVID −19 pandemic, many questions emerged about the transmissibility of SARS-CoV-2, and water was considered as one of the transmission routes. Since some studies have confirmed the presence of infectious coronaviruses in water and wastewater samples, it is important to investigate alternative treatment methods that could complement conventional treatment methods and be used when needed. In this study, the effects of an advanced oxidation process - hydrodynamic cavitation - on phi6 virus were systematically investigated. The main conclusions from the study are as follows:

1. Experiments performed under increasing sample temperature during cavitation resulted in a high, 5.78-log reduction of phi6 after 1000 cavitation passes. The experiments suggest that mechanical effects of cavitation are the main cause of the observed inactivation, but chemical effects cannot be excluded with certainty.
2. Two sets of control experiments indicated that temperature around 30 °C affected virus inactivation, so further experiments were performed at constant sample temperature.
3. The constant sample temperature experiments resulted in a reduction of phi6 by up to 6.3 logs at 30 °C. They showed that inactivation at 10 and 20 °C was predominantly due to mechanical effects of cavitation, while at 30 °C the lipid envelope of phi6 was affected, increasing its susceptibility to inactivation. RNA degradation results confirmed this, as no degradation was detectable.
4. Additional control experiments showed that elevated temperature alone is not sufficient for pronounced virus inactivation, but that some mechanical stress is also required.
5. Hydrodynamic cavitation has the potential to be used as an extension of water treatment systems for inactivation of enveloped viruses at environmentally relevant temperatures.

CRediT authorship contribution statement

Mojca Zupanc: Conceptualization, Data curation, Writing - original draft, Writing - review & editing. **Jure Zevnik:** Formal analysis, Visualization, Writing - original draft. **Arijana Filipić:** Methodology, Writing - original draft. **Ion Gutierrez-Aguirre:** Methodology, Writing - Review & Editing. **Meta Ješelnik:** Investigation. **Tamara Košir:** Investigation. **Jernej Ortar:** Investigation, Visualization. **Matevž Dular:** Writing - review & editing. **Martin Petkovšek:** Conceptualization, Writing - original draft, Writing - review & editing.

Declaration of Competing Interest

The authors declare that they have no known competing financial interests or personal relationships that could have appeared to influence the work reported in this paper.

Acknowledgements

This work was supported by the Slovenian Research Agency (Research Core Funding No. P4-0407, P2-0401, P2-0422, Projects No. L4-9325, J7-1814, J2-3044 and J2-4480), Ministry of Agriculture, Forestry and Food, Domžale-Kamnik Wastewater Treatment Plant and the European Research Council (ERC) under the European Union's Framework Program for research and innovation, Horizon 2020 (grant agreement No. 771567 — CABUM).

Appendix A. Supplementary data

Supplementary data to this article can be found online at https://doi.org/10.1016/j.ultsonch.2023.106400.

References

[1] A.I. Silverman, A.B. Boehm, Systematic Review and Meta-Analysis of the Persistence of Enveloped Viruses in Environmental Waters and Wastewater in the Absence of Disinfectants, Environ. Sci. Technol. 55 (2021) 14480–14493, https://doi.org/10.1021/acs.est.1c03977.
[2] J.A. Jackman, Antiviral peptide engineering for targeting membrane-enveloped viruses: Recent progress and future directions, Biochim. Biophys. Acta - Biomembr. 1864 (2) (2022) 183821.
[3] N. Aquino De Carvalho, E.N. Stachler, N. Cimabue, K. Bibby, Evaluation of Phi6 Persistence and Suitability as an Enveloped Virus Surrogate, Environ. Sci. Technol. 51 (2017) 8692–8700, https://doi.org/10.1021/acs.est.7b01296.
[4] L.M. Casanova, S.R. Weaver, Inactivation of an enveloped surrogate virus in human sewage, Environ. Sci. Technol. Lett. 2 (2015) 76–78, https://doi.org/10.1021/acs.estlett.5b00029.

[5] J. Kong, Y. Lu, Y. Ren, Z. Chen, M. Chen, The virus removal in UV irradiation, ozonation and chlorination, Water Cycle 2 (2021) 23–31, https://doi.org/10.1016/j.watcyc.2021.05.001.

[6] A. Bhatt, P. Arora, S.K. Prajapati, Occurrence, fates and potential treatment approaches for removal of viruses from wastewater: A review with emphasis on SARS-CoV-2, J. Environ. Chem. Eng. 8 (2020), 104429, https://doi.org/10.1016/j.jece.2020.104429.

[7] M. Gomes, M. Bartolomeu, C. Vieira, A.T.P.C. Gomes, M.A.F. Faustino, M.G.P.M. S. Neves, A. Almeida, Photoinactivation of Phage Phi6 as a SARS-CoV-2 Model in Wastewater: Evidence of Efficacy and Safety, Microorganisms. 10 (2022), https://doi.org/10.3390/microorganisms10030659.

[8] J. Li, J. Liu, H. Yu, W. Zhao, X. Xia, S. You, J. Zhang, H. Tong, L. Wei, Sources, fates and treatment strategies of typical viruses in urban sewage collection/treatment systems: A review, Desalination. 534 (2022), 115798, https://doi.org/10.1016/j.desal.2022.115798.

[9] Y. Ye, R.M. Ellenberg, K.E. Graham, K.R. Wigginton, Survivability, Partitioning, and Recovery of Enveloped Viruses in Untreated Municipal Wastewater, Environ. Sci. Technol. 50 (2016) 5077–5085, https://doi.org/10.1021/acs.est.6b00876.

[10] M. Mousazadeh, I. Kabdaşlı, S. Khademi, M.A. Sandoval, S.P. Moussavi, F. Malekdar, V. Gilhotra, M. Hashemi, M.H. Dehghani, A critical review on the existing wastewater treatment methods in the COVID-19 era: What is the potential of advanced oxidation processes in combatting viral especially SARS-CoV-2? J. Water Process Eng. 49 (2022) https://doi.org/10.1016/j.jwpe.2022.103077.

[11] V. Moresco, D.M. Oliver, M. Weidmann, S. Matallana-Surget, R.S. Quilliam, Survival of human enteric and respiratory viruses on plastics in soil, freshwater, and marine environments, Environ. Res. 199 (2021), 111367, https://doi.org/10.1016/j.envres.2021.111367.

[12] K.R. Wigginton, Y. Ye, R.M. Ellenberg, Emerging investigators series: The source and fate of pandemic viruses in the urban water cycle, Environ. Sci. Water Res. Technol. 1 (2015) 735–746, https://doi.org/10.1039/c5ew00125k.

[13] W. Randazzo, P. Truchado, E. Cuevas-Ferrando, P. Simón, A. Allende, G. Sánchez, SARS-CoV-2 RNA in wastewater anticipated COVID-19 occurrence in a low prevalence area, Water Res. 181 (2020), https://doi.org/10.1016/j.watres.2020.115942.

[14] Y. Xu, X. Li, B. Zhu, H. Liang, C. Fang, Y. Gong, Q. Guo, X. Sun, D. Zhao, J. Shen, H. Zhang, H. Liu, H. Xia, J. Tang, K. Zhang, S. Gong, Characteristics of pediatric SARS-CoV-2 infection and potential evidence for persistent fecal viral shedding, Nat. Med. 26 (2020) 502–505, https://doi.org/10.1038/s41591-020-0817-4.

[15] W. Zhang, R.H. Du, B. Li, X.S. Zheng, X. Lou Yang, B. Hu, Y.Y. Wang, G.F. Xiao, B. Yan, Z.L. Shi, P. Zhou, Molecular and serological investigation of 2019-nCoV infected patients: implication of multiple shedding routes, Emerg. Microbes Infect. 9 (2020) 386–389, https://doi.org/10.1080/22221751.2020.1729071.

[16] N. Cahill, D. Morris, Recreational waters – A potential transmission route for SARS-CoV-2 to humans? Sci. Total Environ. 740 (2020), 140122 https://doi.org/10.1016/j.scitotenv.2020.140122.

[17] A. Fedorenko, M. Grinberg, T. Orevi, N. Kashtan, Survival of the enveloped bacteriophage Phi6 (a surrogate for SARS-CoV-2) in evaporated saliva microdroplets deposited on glass surfaces, Sci. Rep. 10 (2020) 1–10, https://doi.org/10.1038/s41598-020-79625-z.

[18] B. Ma, Y.S. Linden, P.M. Gundy, C.P. Gerba, M.D. Sobsey, K.G. Linden, Inactivation of coronaviruses and phage Phi6 from irradiation across UVC wavelengths, Environ. Sci. Technol. Lett. 8 (2021) 425–430, https://doi.org/10.1021/acs.estlett.1c00178.

[19] Á. Serrano-Aroca, Antiviral Characterization of Advanced Materials: Use of Bacteriophage Phi 6 as Surrogate of Enveloped Viruses Such as SARS-CoV-2, Int. J. Mol. Sci. 23 (2022), https://doi.org/10.3390/ijms23105335.

[20] A.J. Prussin, D.O. Schwake, K. Lin, D.L. Gallagher, L. Buttling, L.C. Marr, Survival of the enveloped virus Phi6 in droplets as a function of relative humidity, absolute humidity, and temperature, Appl. Environ. Microbiol. 84 (2018), https://doi.org/10.1128/AEM.00551-18.

[21] A.I. Silverman, A.B. Boehm, Systematic Review and Meta-Analysis of the Persistence and Disinfection of Human Coronaviruses and Their Viral Surrogates in Water and Wastewater, Environ. Sci. Technol. Lett. 7 (2020) 544–553, https://doi.org/10.1021/acs.estlett.0c00313.

[22] B. Karaböce, E. Saban, A. Aydın Böyük, H. Okan Durmuş, R. Hamid, A. Baş, Inactivation of viruses on surfaces by infrared techniques, Int. J. Therm. Sci. 179 (2022), https://doi.org/10.1016/j.ijthermalsci.2022.107595.

[23] Y. Ye, P.H. Chang, J. Hartert, K.R. Wigginton, Reactivity of Enveloped Virus Genome, Proteins, and Lipids with Free Chlorine and UV254, Environ. Sci. Technol. 52 (2018) 7698–7708, https://doi.org/10.1021/acs.est.8b00824.

[24] K. Molan, R. Rahmani, D. Krklec, M. Brojan, D. Stopar, Phi 6 Bacteriophage Inactivation by Metal Salts, Metal Powders, and Metal Surfaces, Viruses. (2022) 1–12. 10.1002/0470009403.ch3.

[25] Z.C. Pope, C. Weisend, A. Shah, H. Ebihara, S. Rizza, Inactivation of Replication-Competent SARS-CoV-2 on Common Surfaces by Disinfectants, Infect. Control Hosp. Epidemiol. 2 (2022) 1–3, https://doi.org/10.1017/ice.2021.527.

[26] M.E.R. Darnell, K. Subbarao, S.M. Feinstone, D.R. Taylor, Inactivation of the coronavirus that induces severe acute respiratory syndrome, SARS-CoV, J. Virol. Methods. 121 (2004) 85–91, https://doi.org/10.1016/j.jviromet.2004.06.006.

[27] S.S. Subhash, M. Cavaiuolo, L.J. Radonovich, A. Eagan, M.L. Lee, S. Campbell, R. A. Martinello, Effectiveness of Common Healthcare Disinfectants against H1N1 Influenza Virus on Reusable Elastomeric Respirators, Infect. Control Hosp. Epidemiol. 35 (7) (2014) 894–897.

[28] S. Smither, A. Phelps, L. Eastaugh, S. Ngugi, L. O'Brien, A. Dutch, M.S. Lever, Effectiveness of four disinfectants against ebola virus on different materials, Viruses. 8 (2016) 1–10, https://doi.org/10.3390/v8070185.

[29] D.H. Morris, K.C. Yinda, A. Gamble, F.W. Rossine, Q. Huang, T. Bushmaker, R. J. Fischer, M. Jeremiah Matson, N. van Doremalen, P.J. Vikesland, L.C. Marr, V. J. Munster, J.O. Lloyd-Smith, Mechanistic theory predicts the effects of temperature and humidity on inactivation of sars-cov-2 and other enveloped viruses, Elife. 10 (2021) 1–59, https://doi.org/10.7554/ELIFE.65902.

[30] V. Soni, A. Khosla, P. Singh, V.H. Nguyen, Q. Van Le, R. Selvasembian, C. M. Hussain, S. Thakur, P. Raizada, Current perspective in metal oxide based photocatalysts for virus disinfection: A review, J. Environ. Manage. 308 (2022), 114617, https://doi.org/10.1016/j.jenvman.2022.114617.

[31] R.B. Martins, I.A. Castro, M. Pontelli, J.P. Souza, T.M. Lima, S.R. Melo, J.P. Z. Siqueira, M.H. Caetano, E. Arruda, M.T.G. de Almeida, SARS-CoV-2 Inactivation by Ozonated Water: A Preliminary Alternative for Environmental Disinfection, Ozone Sci. Eng. 43 (2021) 108–111, https://doi.org/10.1080/01919512.2020.1842998.

[32] R. Djellabi, N. Basilico, S. Delbue, S. D'alessandro, S. Parapini, G. Cerrato, E. Laurenti, E. Falletta, C.L. Bianchi, Oxidative inactivation of sars-cov-2 on photoactive agnps@tio2 ceramic tiles, Int. J. Mol. Sci. 22 (2021), https://doi.org/10.3390/ijms22168836.

[33] N. Mehle, M. Ravnikar, Plant viruses in aqueous environment - Survival, water mediated transmission and detection, Water Res. 46 (2012) 4902–4917, https://doi.org/10.1016/j.watres.2012.07.027.

[34] Y. Benito, S. Arrojo, G. Hauke, P. Vidal, Hydrodynamic Cavitation as a low-cost AOP for wastewater treatment : preliminary results and a new design approach, WIT Trans. Ecol. Environ. 80 (2005) 495–503.

[35] K.S. Suslick, N.C. Eddingsaas, D.J. Flannigan, S.D. Hopkins, H. Xu, Extreme conditions during multibubble cavitation: Sonoluminescence as a spectroscopic probe, Ultrason. Sonochem. 18 (2011) 842–846, https://doi.org/10.1016/j.ultsonch.2010.12.012.

[36] X. Su, S. Zivanovic, D.H. D'Souza, Inactivation of human enteric virus surrogates by high-intensity ultrasound, Foodborne Pathog. Dis. 7 (2010) 1055–1061, https://doi.org/10.1089/fpd.2009.0515.

[37] J. Kosel, I. Gutiérrez-Aguirre, N. Rački, T. Dreo, M. Ravnikar, M. Dular, Efficient inactivation of MS-2 virus in water by hydrodynamic cavitation, Water Res. 124 (2017) 465–471, https://doi.org/10.1016/j.watres.2017.07.077.

[38] A. Filipić, T. Lukežič, K. Bačnik, M. Ravnikar, M. Ješelnik, T. Košir, M. Petkovšek, M. Zupanc, M. Dular, I.G. Aguirre, Hydrodynamic cavitation efficiently inactivates potato virus Y in water, Ultrason. Sonochem. 82 (2022), https://doi.org/10.1016/j.ultsonch.2021.105898.

[39] M. Zupanc, T. Kosjek, M. Petkovšek, M. Dular, B. Kompare, B. Širok, Ž. Blažeka, E. Heath, Removal of pharmaceuticals from wastewater by biological processes, hydrodynamic cavitation and UV treatment, Ultrason. Sonochem. 20 (2013) 1104–1112, https://doi.org/10.1016/j.ultsonch.2012.12.003.

[40] O. Plohl, K. Fric, A. Filipi, First Insights into the Antiviral Activity of Chitosan-Based Bioactive Polymers towards the Bacteriophage Phi6:, (2022).

[41] M. Zupanc, M. Petkovšek, J. Zevnik, G. Kozmus, A. Šmid, M. Dular, Anomalies detected during hydrodynamic cavitation when using salicylic acid dosimetry to measure radical production, Chem. Eng. J. 396 (2020), https://doi.org/10.1016/j.cej.2020.125389.

[42] M. Ge, M. Petkovšek, G. Zhang, D. Jacobs, O. Coutier-Delgosha, Cavitation dynamics and thermodynamic effects at elevated temperatures in a small Venturi channel, Int. J. Heat Mass Transf. 170 (2021), 120970, https://doi.org/10.1016/j.ijheatmasstransfer.2021.120970.

[43] M. Dular, Hydrodynamic cavitation damage in water at elevated temperatures, Wear. 346–347 (2016) 78–86, https://doi.org/10.1016/j.wear.2015.11.007.

[44] S.L. Rath, M. Tripathy, N. Mandal, How Does Temperature Affect the Dynamics of SARS-CoV-2 M Proteins? Insights from Molecular Dynamics Simulations, J. Membr. Biol. 255 (2022) 341–356, https://doi.org/10.1007/s00232-022-00244-y.

[45] I.V. Polozov, L. Bezrukov, K. Gawrisch, J. Zimmerberg, Progressive ordering with decreasing temperature of the phospholipids of influenza virus, Nat. Chem. Biol. 4 (2008) 248–255, https://doi.org/10.1038/nchembio.77.

[46] Ž. Pandur, I. Dogsa, M. Dular, D. Stopar, Liposome destruction by hydrodynamic cavitation in comparison to chemical, physical and mechanical treatments, Ultrason. Sonochem. 61 (2020), 104826, https://doi.org/10.1016/j.ultsonch.2019.104826.

[47] J. Zevnik, M. Dular, Liposome destruction by a collapsing cavitation microbubble: A numerical study, Ultrason. Sonochem. 78 (2021), 105706, https://doi.org/10.1016/j.ultsonch.2021.105706.

[48] Ž. Pandur, M. Dular, R. Kostanjšek, D. Stopar, Bacterial cell wall material properties determine E. coli resistance to sonolysis, Ultrason. Sonochem. 83 (2022), https://doi.org/10.1016/j.ultsonch.2022.105919.

[49] J. Zevnik, M. Dular, Cavitation bubble interaction with compliant structures on a microscale: A contribution to the understanding of bacterial cell lysis by cavitation treatment, Ultrason. Sonochem. 87 (2022), 106053, https://doi.org/10.1016/J.ULTSONCH.2022.106053.